20

Capturing Spatiotemporal Variation in Wildfires for Improving Postwildfire Debris-Flow Hazard Assessments

Jessica R. Haas,[1] Matthew Thompson,[1] Anne Tillery,[2] and Joe H. Scott[3]

ABSTRACT

Wildfires can increase the frequency and magnitude of catastrophic debris flows. Integrated, proactive natural-hazard assessment would therefore characterize landscapes based on the potential for the occurrence and interactions of wildfires and postwildfire debris flows. This chapter presents a new modeling effort that can quantify the variability surrounding a key input to postwildfire debris-flow modeling, the amount of watershed burned at moderate to high severity, in a prewildfire context. The use of stochastic wildfire simulation captures variability surrounding the timing and location of ignitions, fire weather patterns, and ultimately the spatial patterns of watershed area burned. Model results provide for enhanced estimates of postwildfire debris-flow hazard in a prewildfire context, and multiple hazard metrics are generated to characterize and contrast hazards across watersheds. An area in northern New Mexico, USA, is presented as a case-study location, where postwildfire debris flows are a salient hazard and where land managers are actively pursuing mitigation efforts. Modeling results are described in terms of informing mitigation efforts. Limitations and future directions are presented.

20.1. INTRODUCTION

Wildfires and debris flows are two natural hazards that can occur in overlapping geographic areas. Debris flows are a high-density mix of water, soil, rocks, and debris that may have enormous destructive power with potentially catastrophic outcomes. Large, severe wildfires can pose serious threats to human communities, from the destruction of natural and built infrastructure within the fire perimeter to the degradation of watershed health and water supplies, as well as damage to other water-related infrastructure of downstream cities. The ecological and economic impacts of wildfires and debris flows on values, such as clean surface water, may continue for many years after the event occurs, as is evident from the Hayman fire in Colorado [*Rhoades et al.*, 2011] and the Las Conchas and Cerro Grande fires in New Mexico [*Harpold et al.*, 2014; *China et al.*, 2013].

Wildfires can increase the probability and magnitude of a subsequent debris flow for several years after the fire event, with most postwildfire debris flows occurring within the first 2 yr following a wildfire [*Cannon et al.*, 2011; *Smith et al.*, 2011]. The joint probability of a wildland fire event followed by a debris flow is driven by many factors. The wildfire potential is primarily a factor of weather, fuel characteristics of the landscape, and topography [*Parks et al.*, 2011]. The postwildfire debris-flow potential is a function of the percent area of a watershed that burned at moderate to high severity (MHS), the topography and soil characteristics of the watershed, and the intensity and duration of a rainfall event [*Cannon et al.*, 2010]. Burn severity is a measure of the relative changes in prewildfire and postwildfire vegetation cover [*Parsons et al.*, 2002; *Keeley,* 2009]. In recently burned areas, soils, especially on steep slopes, can be highly erodible

[1] *Rocky Mountain Research Station, US Forest Service, Missoula, Montana, USA*

[2] *US Geological Survey, Albuquerque, New Mexico, USA*

[3] *Pyrologix LLC, Missoula, Montana, USA*

Natural Hazard Uncertainty Assessment: Modeling and Decision Support, Geophysical Monograph 223, First Edition.
Edited by Karin Riley, Peter Webley, and Matthew Thompson.

because of decreased vegetation coverage, which increases sediment-laden runoff [*Cannon and Gartner*, 2005]. It is the progressive accumulation of sediment-laden runoff that triggers postwildfire debris flows, rather than discrete slope failure [*Meyer and Wells*, 1997; *Cannon et al.*, 2001].The potential for postwildfire debris-flow initiation changes through time as a function of the rate of vegetation recovery, as well as the timing and intensity of rainfall storms in the area.

Postwildfire debris flows are particularly dangerous because they can be generated in areas that were previously stable and/or in response to rainstorms that would otherwise be considered typical for an area [*Cannon et al.*, 2008]. For example, following the 2003 Grand Prix and Old fires in San Bernardino County, California, 16 people died and mountain roads were cut off by postwildfire debris flows initiated from a typical rainstorm [*Chong et al.*, 2004]. Given the threat to human life, property, and highly valued resources from wildland fires and postwildfire debris flows, there is expanding interest in identifying efficient opportunities to prioritize hazard and risk mitigation efforts [*Warziniack and Thompson*, 2013; *Nature Conservancy,* 2014]. In a postwildfire environment, hazard and risk mitigation efforts typically focus on watershed rehabilitation and soil stabilization [*DeGraff et al.*, 2007]. In these contexts, the extent, location, and severity of the wildfire event is observable, and managers can use predictive models of debris-flow probabilities and volumes to prioritize rehabilitation efforts within and across affected watersheds. These efforts, however, can be challenging because of uncertainty regarding storm patterns, among other factors [*Nyman et al.*, 2013].

Planning and prioritizing mitigation measures becomes even more challenging in a prewildfire environment, because of added uncertainty regarding the location, extent, and severity of wildfire within and across watersheds susceptible to postwildfire debris flows. Nevertheless, prewildfire hazard assessments are a critical component in risk management, especially for prioritizing preventative investments such as hazardous fuel reduction [*Thompson and Calkin*, 2011]. Fuel management, including thinning overly dense forests to reduce wildfire hazard and risk, is often a priority for land managers. While predicting the precise location of a wildfire is impossible, it is possible to identify areas where treatments are likely to be more effective at reducing wildfire hazard and risk.

An integrated hazard assessment would ideally take into account possible interactions of wildfires with postwildfire debris flows, and present a more accurate picture of threats across a landscape. Most research, however, has focused on assessing wildfire and debris-flow hazards individually (although see *Jones et al.* [2014]; *Tillery et al*. [2014], for counterexamples). Wildfire hazard and risk assessments are increasingly used in a wide range of geographic settings and planning contexts [*Haas et al.*, 2013; *Thompson et al.*, 2013a; *Thompson et al.*, 2015a], including watershed-specific wildfire risk [*Thompson et al*., 2013b; *State of California Sierra Nevada Conservancy*, 2014], to predict the likelihood, intensity, and consequences of wildfire across a landscape. Likewise, researchers often use postwildfire debris-flow hazard assessments to map the likelihood and volume of a debris flow from a given watershed, after a wildland fire has already occurred [*Tillery et al.*, 2011; *Staley*, 2013; see also http://landslides.usgs.gov/hazards/postfire_debrisflow/]. In existing models, the primary variable connecting a wildfire and a subsequent debris flow is the amount of a watershed that burns with MHS [*Cannon et al.*, 2010]. This relationship therefore forms the centerpiece of the current modeling effort, building directly from recent work using simulated fire perimeters [*Thompson et al.*, 2013c; *Ager et al*., 2014; *Haas et al*., 2014; *Scott et al*., 2015; *Thompson et al*., 2015b]. Here we use fire perimeters to generate distributions of watershed area burned, and link these outputs with spatially resolved estimates of burn severity to generate distributions of watershed area burned at MHS.

The objective of this chapter is to develop and apply an integrated modeling framework that can be used to support postwildfire debris-flow hazard assessment and mitigation prioritization, before a wildfire occurs. The major methodological innovation is modeling the sizes, shapes, locations, and burn severity patterns of thousands of wildfires, and subsequently treating each as an observed wildfire event with which to estimate postwildfire debris flow probability and volume. As a case study, we apply the framework to seven watersheds on a real-world landscape in northern New Mexico, USA. We demonstrate how this framework can provide information on which watersheds might pose the most serious postwildfire debris-flow hazard, and ultimately to support decisions related to hazard and ultimately risk mitigation. To conclude, we discuss applications, strengths, limitations, and future research opportunities.

20.2. METHODS

20.2.1. Study Area

Our case study focuses on seven watersheds situated along the western slopes to the northeast of Albuquerque in the Sandia Mountains, hereafter referred to as the "Sandias." The watersheds used in this study were delineated from major drainages into watersheds no larger than approximately 11 km^2, the maximum size represented with reasonable confidence in the original database [*Gartner et al.*, 2005] used to generate the *Cannon et al*. [2010] model used in this study (Table 20.1; see Section 20.2.5).

Table 20.1 Watershed Inputs for Debris-Flow Model

Watershed ID	Area (km^2)	Percentage of area with slope ≥ 30%	Ruggedness	Percent clay content	Liquid limit
1	7.17	70	0.54	21.1	26.2
2	0.7	29	0.57	9.4	23.0
3	1.44	22	0.43	9.4	23.0
4	1.52	66	0.79	21.1	26.2
5	2.42	34	0.41	9.4	23.0
6	8	68	0.49	21.1	26.2
7	11.09	64	0.38	21.1	26.2

These watersheds drain directly into communities surrounding the City of Albuquerque, and therefore the threat of wildfire and postwildfire debris flows within them are of particular concern. Figure 20.1 depicts the location of the seven study watersheds, as well as the location of critical water infrastructure. These watersheds vary in terms of size, topography, and soil characteristics used in the debris-flow models.

Vegetation type follows an elevation gradient, beginning with grassland at the lowest elevations and transitioning into pinyon-juniper woodland, ponderosa pine dominated forests, and finally spruce-fir forests at the highest elevations [*Julyan and Stuever*, 2005]. The terrain tends to be steep in this area, with slopes greater than 30% accounting for an average of half of the areal extent of the seven basins. The Sandias have not experienced any large wildfires in recent years. The latest fire of substantial size was in 2011, and burned only 42 acres [*Shor*t, 2014]. The Monitoring Trends in Burn Severity (MTBS) dataset [*Eidenshink et al*., 2007; *US Geological Survey and USDA Forest Service*, 2013] indicates no fires within the Sandias that were over 1000 acres during the period from 1984 to 2011. Because of the lack of recent large fires or disturbances, the vegetation structure of the area is tending toward late succession, which is characterized by an increase in surface and crown fuels [*Keane et al.*, 2000]. Under the right weather conditions, the fuel buildup could lead to a wildfire that would be difficult to suppress given the steep terrain.

20.2.2. Modeling Framework

Figure 20.2 presents the conceptual overview of postwildfire debris-flow modeling framework. The primary output of interest is the estimation of postwildfire debris-flow probability and volume, but our primary modeling interest is to better capture wildfire–debris-flow hazard interactions. Starting from the upper right of Figure 20.2, landscape conditions relating to watershed size, topography, and soil characteristics are held constant as inputs into the debris-flow model. For reasons described below, the spatial pattern of potential burn severity is also held constant. The upper left side of Figure 20.2 describes the inputs that vary in modeling the postwildfire debris flows. Stochastic simulation is used to output fire perimeter polygons (i.e., the wildfire event set), which are then overlain with watershed boundaries to generate distributions of watershed area burned. For each wildfire event, the storm characteristics for six recurrence interval storms were used in the model, resulting in six probabilities and six volumes for each wildfire event. The two grey boxes represent inputs that we modeled using fire behavior and fire perimeter growth models, described below. These four boxes collectively represent inputs to statistical models of debris-flow probability and volume. Last, debris-flow model outputs are analyzed to characterize watershed-level hazards.

20.2.3. Wildfire Modeling

The primary purpose of modeling wildfire in this study is to provide the area of a watershed that could burn at MHS for a set of possible wildfire events. We used two separate fire simulation models to achieve this aim. To generate the sizes, shapes, and locations of simulated perimeters, we used the FSim fire modeling system [*Finney et al.*, 2011]. Unfortunately, because of storage and processing limitations, FSim does not retain information on fire behavior for every simulated perimeter, precluding direct estimation of burn severity. To estimate severity, we instead used the FlamMap [*Finney,* 2006] fire-behavior model. These fire models use the same basic set of landscape inputs, but vary in function and capacity, as described in the following subsections. The primary difference between FlamMap and FSim is that rather than using a single set of fire-behavior outputs for each fire event, FSim invokes FlamMap to generate many possible fire-behavior outputs, based on the historical weather combinations of wind speed, direction, and three levels of fuel dryness as measured by the 80th, 90th, and 97th percentile Energy Release Component (ERC) [*Bradshaw et al.*, 1983; *Finney et al.*, 2011]. Additionally, in FlamMap, fire growth is set for a specific burn period, where with FSim fires may continue to grow for multiple burn periods.

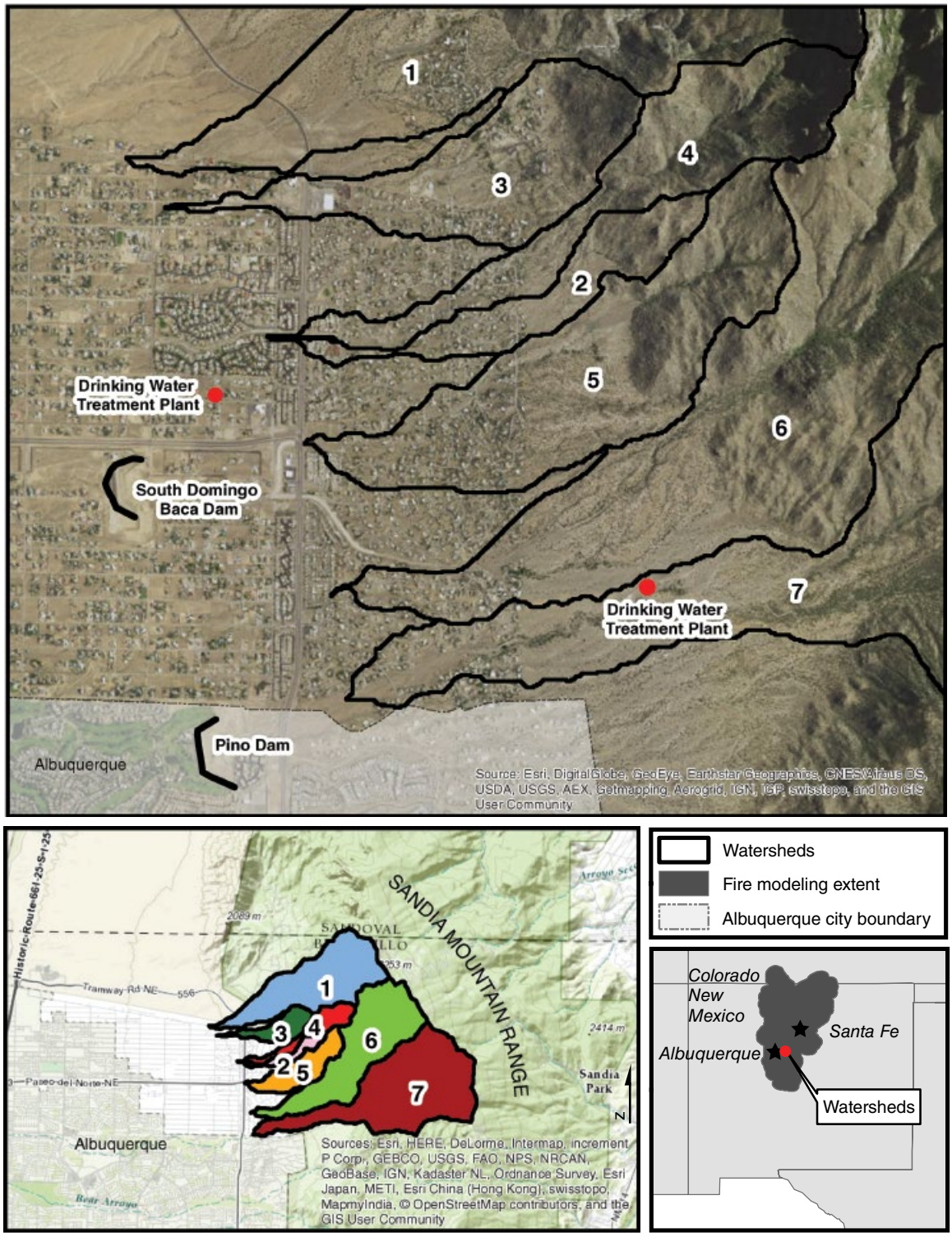

Figure 20.1 Study area with the selected watersheds identified. The top panel shows a zoomed in detailed view of the watershed outlets into the adjacent urban interface, and identifies key water-infrastructure located in the vicinity. In some cases, there is urban development within the watershed itself (i.e., watershed 1). The bottom left panel shows complete delineation of the watersheds and their more general location within the Sandia Mountain range. The color of each watershed corresponds to the colors used to distinguish between watersheds in the results figures. The bottom right panel shows the location of the watersheds with respect to the greater landscape used in modeling the fire inputs.

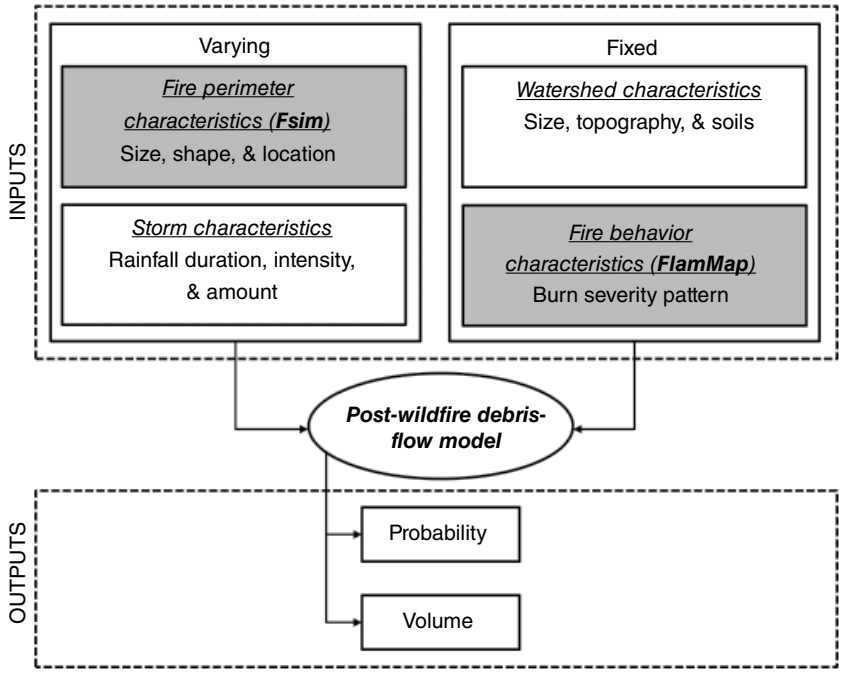

Figure 20.2 Overview of modeling framework, showing linkages between the various models (named in bold), which provides the ultimate outputs characterizing watershed-level risks (debris-flow probability and volume). The two grey boxes represent inputs modeled using fire-behavior and growth models.

20.2.3.1. FSim Modeling: Watershed Area Burned

The FSim model is focused on simulating relatively rare "large" (greater than 100 ha) wildfires that account for a small fraction of total number of fires, but that account for the vast majority of area burned [*Short,* 2013]. The FSim model uses historical information on fire occurrence, weather, and fire suppression efforts to simulate thousands of hypothetical fire seasons. In the simulation, fires are probabilistically ignited according to the relationship between the fire weather and fire occurrence derived from the historical data. Each fire then "grows" in accordance with fire-behavior outputs and Minimum Travel Time fire spread theory [*Finney*, 2002]. Each simulated fire may continue to grow for many burn periods (i.e., days). The fire behavior and growth for each burn period is determined by the fire weather generated for that day and can therefore vary throughout the duration of the fire. The fire continues to burn until it is extinguished by a statistical suppression algorithm [*Finney et al.*, 2009]. The suppression algorithm probabilistically contains fires based on the relationship between large fire containment and duration, fire growth, and fuel type. The landscape size used in the FSim and FlamMap model is much larger than the seven watersheds included in this study. We ran the FSim and FlamMap models on a landscape of 35,000 km ^{2} (Fig. 20.1). In addition to capturing the broader fire occurrence, this larger landscape allows fires to ignite remotely and burn into the watersheds, as well as to ignite within the watersheds and burn out of them.

The outputs are calibrated to historical fire occurrence, in terms of the mean annual area burned and mean number of large fires per year. For this effort, 30,000 unique fire seasons were simulated, with the principal output of interest being the set of final fire perimeters from each simulated season.

20.2.3.2. FlamMap Modeling: Spatial Burn Severity Patterns

Currently, fire-behavior models do not calculate burn severity. However, fire-behavior models do output fire intensity. Fire intensity is the amount of energy released when a fuel burns, and is measured in either kilowatts per meter or as flame height in meters [*Alexander and Cruz*, 2012]. This measure depends primarily on the weather, topography, and fuel characteristics at the time of burning. Through empirical modeling, intensity is used in generating fire-behavior outputs such as rate of spread and crown-fire initiation [*Rothermel,* 1972; *Scott and Burgan*, 2005; *Alexander and Cruz*, 2012]. Intensity is highly correlated with severity, especially in forested landscapes, where high fire intensity will result in crown fire [*Keeley*, 2009]. Crown fire is the movement of fire into and throughout the forest canopy, which results in relatively high levels of vegetation consumption and mortality and is therefore a useful proxy for MHS in forested landscapes.

The fire-behavior model FlamMap [*Finney,* 2006] incorporates spatial information on topography and fuel models, the ERC, and wind data to estimate a single set of fire-behavior outputs, including crown-fire potential. The crown-fire potential is generated spatially on a landscape from a set of topographic and fuel characteristics, collectively known as the landscape file, generated for this study from input data obtained from the LANDFIRE LF 1.3 dataset [*LANDFIRE*, 2012]. These characteristics include slope, elevation, aspect, crown base height, canopy base height, canopy bulk density, canopy coverage, and surface fuel model. We calculated crown-fire potential using the Scott and Reinhardt crown-fire method [*Scott and Reinhardt*, 2001]. Wind inputs were based on the most common combination of historically observed wind speed (16 km/h) and direction (270 degrees) from the same weather inputs used in the FSim model discussed above. We generated the crown-fire potential for the 90th percentile ERC, a measure of fuel moisture. The 90th percentile ERC represents fuel dryness resulting in common fire behavior during large fires, rather than the 97th percentile ERC, which would result in uncommon, extreme fire behavior, or 80th percentile ERC, which represents minimal fire growth and behavior. In forested landscapes, we use the resulting crown-fire potential as a surrogate for MHS.

In nonforested landscapes, such as shrub or grasslands, the surface-fuel model is a better indicator of MHS than crown-fire potential, because these landscapes do not possess a canopy. A surface-fuel model is the complete set of fuel inputs needed to calculate a mathematical representation of fire intensity and wildfire spread [*Rothermel,* 1972]. In grasslands, even a high-intensity fire typically results in low burn severity because of the rapid regeneration of grasses after a fire. Additional studies have shown that grassland fires typically burn under low severity and result in little to no erosion response [*Johansen et al.*, 2001]. Therefore, areas mapped as a grassland surface-fuel model were not considered prone to MHS fire. In shrublands, high-intensity fires are highly correlated with MHS fire [*Pyne et al.*, 1996; *Keeley et al*., 2008]. Because fuel models define the intensity at which the fuel burns, high-intensity shrub-fuel models can be used as a surrogate for MHS fire potential in these communities. The shrub surface fuel models SH5 and SH7, from the Scott and Burgan 40 fire behavior fuel models [*Scott and Burgan*, 2005], have potential for high-intensity fire behavior. We used the presence of these fuel models to identify the areas with potential for MHS in shrublands.

Total MHS fire potential for the study area was calculated as the sum of the predicted crown-fire activity areas and the high-intensity shrub fuel areas. The resulting output was calibrated to observed burn severity using the Monitoring Trends in Burn Severity data [*US Geological Survey and USDA Forest Service*, 2013] for geographically relevant historical fires, based on the methods described in *Tillery et al*. [2014, Appendix]. Crown-fire activity was predicted to occur on approximately 20% of the land area of the seven watersheds; an artifact of relatively high potential for crown fire in timbered areas (66%) across a relatively small share of the landscape (30%). The two shrub-fuel models account for 7% of the watersheds, for a total of 27% of the watersheds having the potential for MHS fire. The remaining shrubs and grasslands, which are the primary vegetation types, tend to carry fast-moving surface fires resulting in a low-severity fire, as discussed above.

20.2.4. Watershed Area Burned at MHS

Figure 20.3 illustrates how fire perimeters and burn-severity patterns are combined and overlaid with watershed perimeters. While the spatial MHS patterns are static within a watershed, the location, shape, and size of each fire perimeter and its relation to watershed boundaries result in an individual calculation of watershed area burned at MHS for every simulated fire. Note that, for this particular landscape, results can exhibit substantial variation in fire size, severity, and watershed area burned. Even when the watershed experiences fire, it is not necessarily the case that the entire watershed burns (although multiple watersheds can be burned by the same fire). Further, even if the entire watershed does burn, MHS does not necessarily occur everywhere. The maximum area of a watershed that can burn with MHS occurs only when a fire perimeter burns the entire watershed, and is then limited by the total area within the watershed mapped as having the potential for MHS. This approach captures the variation surrounding potential future wildfire events with respect to the inputs required for debris-flow modeling.

20.2.5. Debris-Flow Hazard Assessment

Debris-flow modeling efforts use the statistical models for postwildfire debris-flow probability and volume developed by *Cannon et al.* [2010]. The probability of debris-flow occurrence is a function of terrain, soil characteristics, the percentage of the watershed that burned at MHS, and storm intensity. Equation 20.1 is used to calculate debris-flow probability:

$$Probability\left(DF \mid f, s\right) = \frac{e^{x}}{1+e^{x}} \qquad (20.1)$$

where: $Probability\,(DF \mid f, S)$ is the probability of a post-fire debris flow, given a fire event f and a storm event S.

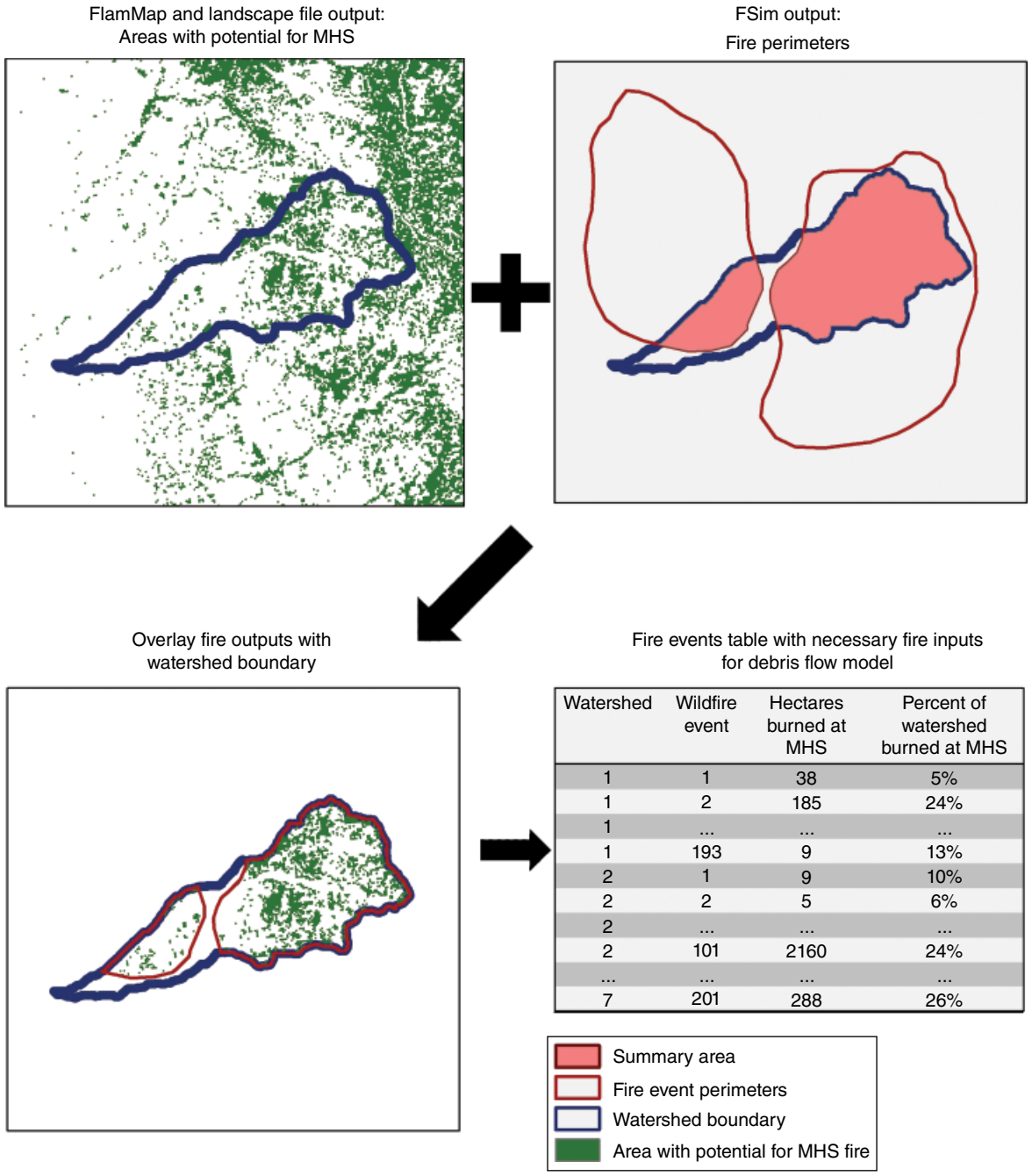

Watershed	Wildfire event	Hectares burned at MHS	Percent of watershed burned at MHS
1	1	38	5%
1	2	185	24%
1	...	...	...
1	193	9	13%
2	1	9	10%
2	2	5	6%
2	...	...	...
2	101	2160	24%
...	...	...	...
7	201	288	26%

Figure 20.3 The depiction of the final step in the methods that produces the necessary fire inputs for the debris-flow model. The spatial intersection of the FlamMap severity output and the FSim fire-perimeter output with watershed boundaries jointly determine the distribution of watershed area and percent burned at MHS.

Equation 20.2 is used to calculate x:

$$x = -0.7 + 0.03(\%SG30) - 1.6(R) + 0.06(\%AB) + 0.07(I) + 0.2(\%C) - 0.4(LL) \quad (20.2)$$

where %SG30 is the percentage of the basin area with a slope equal to or greater than 30%.

R is the basin ruggedness, the change in basin elevation (m) divided by the square root of the basin area (m^2), $\%AB$ is the percentage of basin area burned at MHS, I is the average storm intensity of storm event S, $\%C$ is the percentage clay content of soil, LL is the liquid limit of soil (the percentage of soil moisture by weight at which a solid begins to behave as a liquid).

The potential volume of a debris-flow occurrence is a function of a similar set of variables, but instead considers total watershed area burned at MHS, as well as total storm rainfall. The equation (20.3) for modeling debris-flow volume is:

$$Ln\left(Volume\left(DF\,|\,f,S\right)\right) = 7.2 + 0.6\left(Ln\left(SG30\right)\right) + 0.7\left(AB\right)^{0.5} + 0.2\left(T\right)^{0.5} + 0.3 \quad (20.3)$$

where: $Volume(DF\,|\,f,S)$ is the debris-flow volume (in cubic meters) given fire event f and storm event S; $SG30$ is the area of drainage basin with slopes equal to or greater than 30% (in square kilometers); AB is the drainage basin area burned at MHS (in square kilometers); T is the total storm rainfall (in millimeters) of storm event S; and, 0.3 is a bias correction factor that changes the predicted estimate from a median to a mean value [*Cannon et al.*, 2010; *Helsel and Hirsch*, 2002].

Debris-flow probabilities and volumes were calculated at the watershed outlets or pour points, for each of the 30,000 fire seasons. When a fire burned the watersheds during a simulated fire season, the percent area burned under MHS that was calculated in Section 20.2.4 was used for the $\%AB$ and the AB values needed above.

20.2.6. Characterizing Watershed Integrated Hazard

To characterize watershed-level hazard, we calculated postwildfire debris-flow probability and volume over a range of storm scenarios (Table 20.2). Results are conditional in the sense that they depend on a specific recurrence interval storm. A more complex analysis would simultaneously consider a range of storms and their respective occurrence probabilities, a topic we revisit in the discussion. Because of orographic effects of the mountainous terrain, rainfall totals and rainfall intensities will slightly vary over the extent of the study area. Therefore, for this study, we used the NOAA Atlas 14 gridded precipitation frequency estimates [*Bonnin et al.*, 2004] to derive unique storm intensities for each watershed, for six recurrence interval 30 min duration storms. When more than one gridded value was located in a watershed, we use the maximum precipitation value within the watershed for each recurrence interval, providing the most conservative, or highest, estimate of storm intensity and amount. Table 20.2 shows the range of storm intensities across the watersheds for the recurrence intervals.

20.3. RESULTS

20.3.1. Wildfire Simulation Results

We calibrated the FSim run to match historical rates of annual hectares burned and mean number of large fires per year. Across the study area landscape, the FSim wildfire simulation burned an average of 10,090 ha annually, relative to the historical average of 9,636 ha [*Short,* 2014]. We simulated an average of 4.3 large fires per year, compared with the historical average of 4.9 large fires per year [*Short,* 2014]. The majority of the simulated fire seasons did not produce a wildfire that burned any portion of any of the watersheds, meaning the precursor event to a postwildfire debris flow is rare (Table 20.3). Only 280 fires burned at least a portion of one of the watersheds, and there were no seasons with multiple fires burning in the watersheds. Out of 30,000 simulated fire seasons, the watershed that experienced the most wildfires (WS7) only experienced 201 wildfire events, which equates to a 0.07% chance of at least a portion of the watershed burning annually. The maximum percentage of a watershed that burned at MHS ranged from 6.5% (WS2) to 36.0% (WS7), and the mean ranged from 3.2% (WS1) to 16.5% (WS7).

20.3.2. Postwildfire Debris-Flow Results

Figure 20.4 presents scatterplots of the individual simulated fire events and their corresponding conditional debris-flow probabilities and volumes, for each of the six storm recurrence intervals. The probabilities and volumes are conditional upon a storm occurrence. Each point on each scatterplot represents an individual wildfire event,

Table 20.2 Attributes of Analysis Recurrence Interval Storms

Recurrence level	Duration (minutes)	Average storm intensity across watersheds (mm/hr)	Range of storm intensities across watersheds (mm/hr)
2 yr	30	34	34–35
5 yr	30	46	45–47
10 yr	30	55	53–55
50 yr	30	76	74–77
100 yr	30	85	84–86
500 yr	30	108	107–109

Note: Storm values are assumed to be constant across each watershed.

Table 20.3 Wildfire Events Summary Data for Each Watershed

Watershed ID	Number of fire events (F)	Percent annual probability of wildfire	Max and mode percent WS burned	Max. and mode percent MHS	Mean percent WS burned	Mean percent MHS
1	193	0.06	100	24.6	51.5	14.4
2	101	0.03	100	6.5	48.1	3.2
3	193	0.06	100	17.2	53.0	9.2
4	129	0.04	100	19.4	58.8	12.7
5	193	0.06	100	13.9	48.5	6.7
6	182	0.06	100	26.4	50.9	15.0
7	201	0.07	100	36.0	44.0	16.5

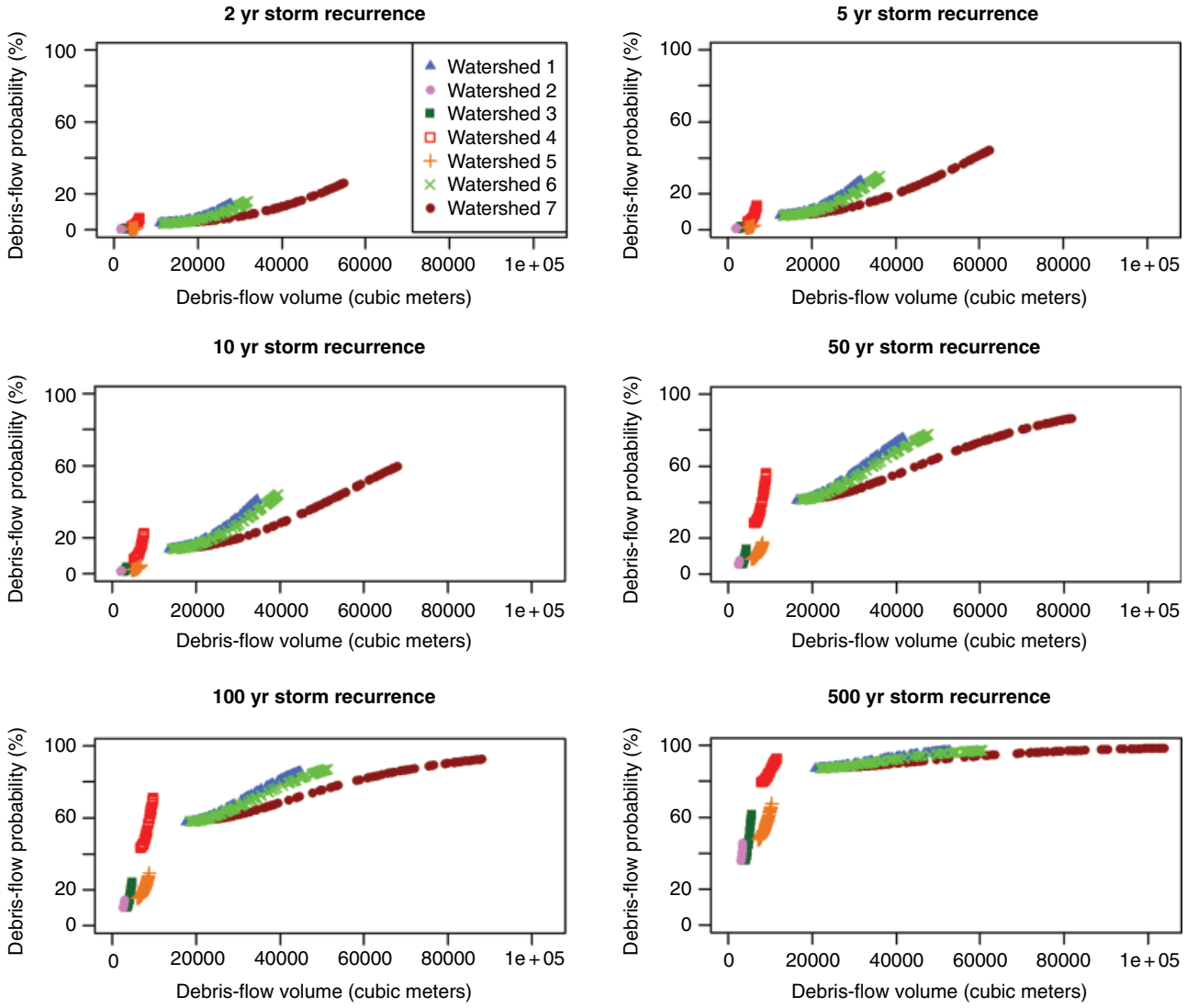

Figure 20.4 Debris-flow probability versus debris-flow volume for the six storm recurrence intervals for each watershed. The individual dots represent the individual fire events associated with each watershed and the range of variability surrounding the potential fire events. Each dot may represent more than one fire event because of the limited spatial combinations of percent area burned at MHS.

and points are colored and grouped by watershed. The colors in Figure 20.4 match those found in the lower left panel of Figure 20.1, for ease of comparison. The variation among events is caused by the simulated differences in the area of a watershed that burned under MHS. Because of the limited combinations of percent area burned at MHS, some perimeters that burned in different locations or with different final fire sizes burned the same proportion of the watershed at MHS, leading to identical debris-flow results (i.e., some points on the scatter plot may actually represent multiple fire events). As storm recurrence intervals increase, the probability and volume of postwildfire debris flows also increase.

For a given debris-flow probability, watershed 7 consistently yielded the largest overall debris-flow volume regardless of storm recurrence level. Watershed 7 also yielded the largest range of variability in debris-flow volume across wildfire events. For a given debris-flow volume, watershed 1 consistently yielded the highest overall debris-flow probability, mirrored closely by watershed 6 and to a lesser extent by watershed 7. Watersheds 2, 3, 4, and 5 tended to yield consistently lower debris-flow probabilities and volumes than watersheds 1, 6, and 7, with watershed 4 presenting the steepest increase in debris-flow probability as storm recurrence interval increased.

How watersheds might be ranked in terms of hazard depends on whether the ranking focuses on debris-flow probability or volume. For example, conditioned upon the 50 yr recurrence interval storm, watersheds 1, 4, 6, and 7 all have a simulated fire event (or set of events) that resulted in a 55% probability of a debris flow. However, the debris-flow volume for each of these watersheds at that probability varies, with watershed 4 having the lowest volume (9,066 m^3) and watershed 7 having almost four times that volume (39,000 m^3). Similarly, for the same recurrence interval, watersheds 1, 6, and 7 all had an event that produced a relatively large-volume debris flow (40,000 m^3). However, the debris-flow probabilities varied between watersheds, with watershed 7 having the lowest likelihood of a 40,000 m^3 debris flow (56%) and watershed 1 having the highest probability of this relatively large-volume debris flow (73%). This example reiterates the need for assessing the range of possible events when analyzing the potential for joint hazards.

Figure 20.5 displays histograms of simulated postwildfire debris-flow volumes for each watershed, for the 50 yr recurrence interval storm. The histogram can better capture variability across the low frequency, large-volume events and the high frequency, small-volume events. This is because, for reasons described above, each point in Figure 20.4 may represent more than one wildfire event thereby masking the total number of simulated postwildfire debris-flow events (see Table 20.3). Examining the watersheds with the greatest probability of debris flows, both watershed 1 and 6 have a similar range of predicted debris-flow volumes, however the frequency distribution of events is slightly different, with watershed 6 primarily having more large volumes events, and watershed 1 having a greater mix of volume events. Watershed 7 again shows the greatest variability where most of the events are either low-volume events or high-volume events, with very few moderate events. Notably, all three watersheds have the highest frequency in the largest volume bin because when a simulated fire burned a portion of a watershed, it most often burned the entire watershed (see Table 20.3). In other words, the maximum event (i.e., worst-case scenario) was the same as the most common event (i.e., the mode event) for all the watersheds in the study area.

While exploring the variation in probability and volume is necessary, providing a single metric of hazard across all simulated events is useful when trying to rapidly identify the watershed with the greatest hazard. This becomes particularly important when evaluating larger landscapes and comparing across a much larger set of watersheds. There are different ways to rank hazards when varying events lead to varying outcomes. One method is to take the ensemble event (the mean event), another is to use the event that occurred most often (the mode event), and yet another is to investigate the worst-case scenario (the maximum event). The reason for choosing one option or another depends on the goals of the researcher or land manager. Using the mode event and the 100 yr recurrence interval storm, watersheds can be ranked from greatest to least hazard as 7, 6, 1, 4, 5, 3, and 2.

Figure 20.6 displays results on wildfire probability, burn severity, and debris-flow probability and volume for each watershed for the 100-year recurrent interval storm. This information helps decompose and graphically display the underlying factors driving hazard assessment in each watershed. Watershed 7 ranked highest for all of the individual components, and clearly presents the greatest hazard consistent with the mode event rankings. Watersheds 1 and 6 have identical estimates of experiencing a large wildfire, and while watershed 6 has a lower area that can burn with MHS, it has slightly greater mode and mean debris-flow probability and volume estimates. This suggests that, relative to wildfire probability and burn severity, differences in watershed size along with soil and topography characteristics may be greater drivers of postwildfire response.

For fuels-mitigation planning, we compare the worst case scenario wildfire event (the maximum area with potential for MHS is burned) to the best case scenario event (none of the watershed area with potential for MHS is burned). The difference between these two events would represent the decrease in debris-flow hazard if fuel treatments could be 100 percent successful in eliminating MHS fire. In reality, this assumption rarely holds true; however, the comparison can give insight as to which

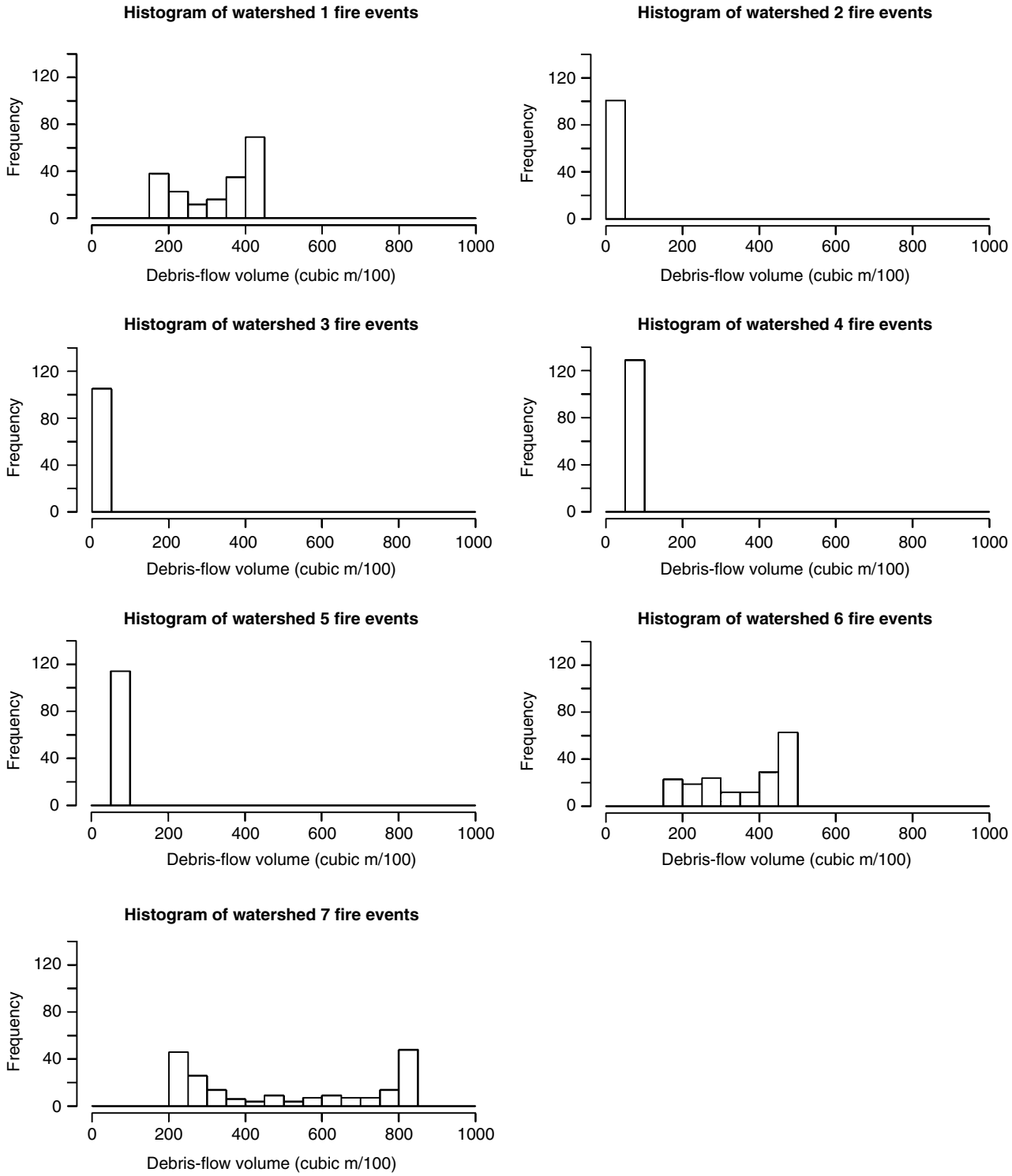

Figure 20.5 Frequency histograms showing distributions of the postwildfire debris-flow volume for the set of fire events. The histograms allow comparison of watershed hazard by frequency of event, which can distinguish watersheds with low-frequency large-volume events from those with high-frequency small-volume events, which can result in similar combined hazard metrics.

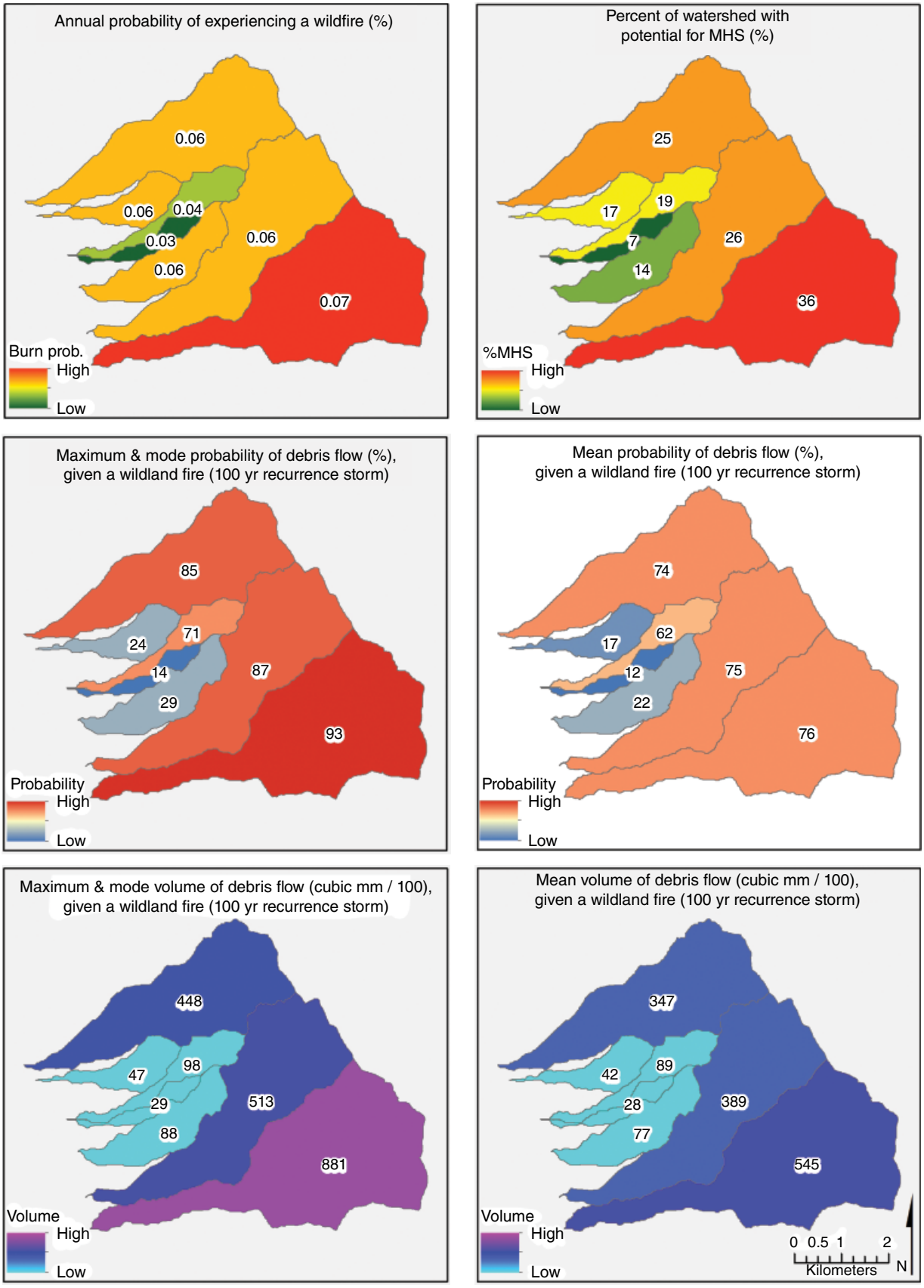

Figure 20.6 The summary statistics for the wildfire events by watershed. The top left panel shows the annual burn probability as a percentage for each watershed. The top right panel shows the percentage of each watershed that would burn at MHS as modeled in this study, if the entire watershed burned. The probability of debris flow (center panels) and volume of debris flow (bottom panels) show the maximum and mode (left, same value for each watershed) and mean (right) values, given a wildfire event. The colors represent the same value between the mean and the mode event for the two variables, allowing for a direct visual comparison between the modal statistics.

Table 20.4 A Comparison of Postwildfire Debris Flow Hazards for the Worst-Case Scenario Event Versus a Best-Case Scenario Event

	Debris-flow probability (percent)				Debris-flow volume (m3)			
	Percentage of area with potential for MHS fire burned		Absolute	Percent	Percentage of area with potential for MHS fire burned		Absolute	Percent
Watershed ID	100%	0%	reduction	reduction	100%	0%	reduction	reduction
1	85%	57%	28	−33%	44,800	27,100	17,700	−40%
2	14%	10%	4	−29%	2,900	400	2,500	−86%
3	24%	10%	14	−58%	4,700	1,300	3,400	−72%
4	71%	44%	27	−38%	9,800	3,200	6,600	−67%
5	29%	15%	14	−48%	8,800	2,800	6,000	−68%
6	87%	58%	29	−33%	51,300	32,700	18,600	−36%
7	93%	59%	34	−37%	88,100	66,400	21,700	−25%

Note: Worst-case scenario event = 100% of area with potential for MHS fire burned; Best-case scenario event = 0% of area with potential for MHS fire burned.

watersheds would see the most reduction in postwildfire debris-flow hazard from fuel treatments designed to reduce severity. By examining the 100-year recurrence interval storm, Table 20.4 shows that if MHS fire could be eliminated from watershed 7 (the watershed with the greatest hazard ranking), debris-flow probability would be reduced from 93 percent to 59 percent, a 37 percent reduction. Additionally, debris-flow volume would be reduced from an estimated 88,100 m^3 to 66,400 m^3, a 25 percent volume reduction. Watershed 2 has the greatest percent reduction for volume (86 percent) and watershed 3 has the greatest percent reduction for probability (58 percent). Using these methods, the maximum event can be compared to other events that match a more realistic expected reduction in MHS fire if fuel treatments were implemented. This reduction would depend on the type and extent of treatment designed. Fuel treatments not only influence the severity of a fire, they influence the rate of spread, and therefore the final fire perimeters. A true analysis of fuel treatment effectiveness would be much more complex and involve incorporating the fuel-treatment effects on not only potential burn severity, but fire spread, fire size, and total watershed area burned. Regardless, the above exercise provides a quick way to assess the reduction of debris-flow hazard, given fuel-treatments designed to eliminate or reduce MHS fire.

20.4. DISCUSSION

This research effort sought to expand the horizons of postwildfire debris-flow modeling in a prewildfire context, with the ultimate aim of providing actionable information that supports hazard-mitigation. The analysis used stochastic simulation to proactively estimate a range of possible wildfire and debris-flow outcomes. In particular, we keyed in on the primary fire-related variable in the debris-flow model (watershed area burned at MHS) and did so by overlaying simulated spatial fire perimeters with modeled burn severity patterns and watershed boundaries. Given the inherent variability in the location and extent of wildfires and their interactions with watersheds, this approach provides critical spatial information on areas of high fire likelihood and severity that can lead to increased debris-flow hazards. We provided a range of hazard metrics that offer a relatively simple and graphically intuitive way to compare multiple hazards across watersheds and under a range of design storms. Our analysis incorporated information on the annual likelihood of a wildfire event, the amount of area in a watershed prone to MHS fire, watershed soil and topography characteristics, and design storm characteristics. Results can guide mitigation efforts by allowing planners to identify which factors may be contributing the most to the hazard rankings of watersheds.

20.4.1. Uncertainties and Limitations

Prediction of the exact timing, location, magnitude, and extent of postwildfire debris flows is inherently difficult if not impossible, and subject to a cascading chain of uncertainties [*Hyde et al.*, Chapter 19, this volume]. Analysis of factors influencing debris-flow initiation, however, can reveal substantial differences in spatial patterns of postwildfire debris-flow probability and volume. Leveraging state-of-the-art spatial fire models with widely used postwildfire debris-flow models can generate useful information for managers who are proactively seeking to understand, prioritize, and mitigate hazards. Hazard modeling results can directly inform mitigation efforts across a variety of planning contexts. Where watershed-level results are highly sensitive to area burned, as was illustrated in some cases, then fuel-treatment planning may focus on strategically locating treatments to interrupt fire spread pathways and/or to increase suppression efficacy. To reduce burn severity, fuel-treatment planning

may target areas likely to experience crown fire. If fuel-treatment opportunities are limited but hazards are sufficiently high, downstream investments in water treatment infrastructure may be the more cost-effective option. In either case, a broader suite of the costs and benefits to values need to be weighed and balanced, such as enhanced ecosystem services from watershed restoration (in the case of forest management) or broadened defense against water-quality effects from other pollutants/stressors (in the case of water-treatment capacity investment). In some if not many cases, the relative rarity of MHS wildfire in any given location coupled with the probabilities of storm occurrence and debris-flow initiation would suggest a low return on investment for hazardous fuels treatments targeted specifically at mitigating debris-flow hazard. In other cases, where factors align to indicate high hazard, debris-flow-mitigation investments may be worthwhile, especially if implemented as part of a broader restoration strategy with other economic and environmental objectives. Capturing information on the low-probability high-consequence events can be particularly informative for evaluating mitigation options.

The modeling approach does have notable limitations, and a number of research directions are evident. The combination of models always carries potential for compounding uncertainty, which in this case would center around burn severity patterns and simulated perimeters fed into the debris-flow model [*Cannon et al.*, 2010]. As described in the results section, fire-modeling results were carefully calibrated, and modeled variation in debris-flow hazard across watersheds appears to capture underlying differences in hazard rather than artifacts of uncertainty in the models. At a basic level, future research directions include expanding the empirical base for modeling debris flows [*Riley et al.*, 2013]. Debris-flow models may misrepresent the hazard because of an imperfect knowledge of the system [*Smith et al.*, 2011] as well as a limited set of empirical observations. This latter concern is particularly relevant as the dataset upon which the *Cannon et al.* [2010] model was built included no observations from the current study area. Although the debris-flow model is being updated with more observations including debris flows in New Mexico, this limitation would nevertheless need to be addressed for any operational use of the modeling framework demonstrated here. Wildfire modeling limitations include knowledge gaps related to fire severity prediction [*Hyde et al.*, 2012] and fire-spread modeling [*Finney et al.*, 2012; *Riley and Thompson*, Chapter 13, this volume].

20.4.2. Future Research Directions

There are at least three logical extensions to the modeling framework developed here: (1) storm-occurrence probabilities, (2) burn-severity probabilities, and (3) risk assessment considering consequences and downstream values. First, while the results here focused on the conditional occurrence of a given storm, future efforts could directly incorporate the distribution of different storm intensities to generate unconditional results, for instance through an expanded Monte Carlo simulation approach. A complete analysis would consist of not only simulating the yearly fire season as done here, but the subsequent storm events for the next 3 yr when postwildfire debris flows are most likely to occur. This would allow for information related to temporal synchronicity of extreme fire weather, followed by extreme rain events to be more fully incorporated into the analysis.

Second, future efforts could adopt a more probabilistic approach to burn severity rather than the static burn-severity potential map used here. A single indicator of burn severity for a given pixel does not capture the true complexity of burn-severity patterns across a landscape. If technical details of fire-modeling systems evolve, it may also be possible to simulate patterns of burn severity for each simulated fire, for instance capturing the possibility for widespread MHS fire under extreme weather conditions. Additionally, modeling the probability and volume of a debris flow in the absence of fire would provide useful information; however, currently there is no model that simulates both prewildfire and postwildfire debris-flow hazard in a consistent manner. If such information were made available, one could decipher how much of the total debris-flow hazard was caused by wildfire compared to the inherent characteristics of the watershed and storm intensity. This information would further guide mitigation efforts.

Last, it would be useful to expand the hazard analysis into a full risk assessment. The risk assessment incorporates information on the impacts from the hazards on values of concern to society. For example, a risk analysis could incorporate the consequences of the wildland fire and the debris flow on measures of population served, the location of water-conveyance infrastructure, and sediment delivery pathways. This type of analysis would need to model sediment transport, as well as the probability and volume of a debris flow. Future efforts in the near term can focus on how to leverage these results into real-world mitigation planning on landscapes in New Mexico and elsewhere. Efforts can also focus on more strongly incorporating temporal elements and underlying forest dynamics, ideally better capturing the spatial and temporal coincidence of burned areas and storms.

20.5. CONCLUSION

This work greatly expands the information available to land managers and planners with hazard-mitigation duties by providing a richer way of investigating the

variability surrounding the integration of multiple hazards, and a method for comparing hazards across watersheds. By mitigating the negative effects of postwildfire debris flows before a fire occurs, communities can better prepare for the natural hazards that occur in their area, and ultimately reduce the risks associated with these hazards. Under limited time and budgets, our work can help identify watersheds that have the highest combined hazard, and therefore aid in prioritizing where mitigation efforts would be the most beneficial. This work has already informed stakeholders involved in the Rio Grande Water Fund of the postwildfire debris-flow hazards in the Sandia Mountain area. Additional work will expand the analysis area north to include the Jemez and Sangre de Cristo mountains of New Mexico, to better capture the risk of postwildfire debris flows on the Rio Grande watershed.

REFERENCES

Ager, A. A., M. A. Day, M. A. Finney, K. Vance-Borland, and N. M. Vaillant (2014), Analyzing the transmission of wildfire exposure on a fire-prone landscape in Oregon, USA, *For. Ecol. Man.*, *334*, 377–390.

Alexander, M. E., and M. G. Cruz (2012), Interdependencies between flame length and fireline intensity in predicting crown fire initiation and crown scorch height, *Int. J. Wildland Fire*, *21*, 95–113.

Bonnin, G. M., D. Martin, B. Lin, T. Parzybok, M. Yekta, and D. Riley (2004), Precipitation-frequency atlas of the United States, Volume 1 Version 5.0, Semiarid Southwest (Arizona, Southeast California, Nevada, New Mexico, Utah), National Oceanic and Atmospheric Administration Atlas 14, National Oceanic and Atmospheric Administration, Silver Spring, MD, 271.

Bradshaw, L. S., R. E. Burgan, J. D. Cohen, and J. E. Deeming (1983), The 1978 National Fire Danger Rating System: Technical documentation, USDA Forest Service; Intermountain Forest and Range Experiment Station, General Technical Report INT-169, Ogden, UT.

Cannon, S. H., and J. E. Gartner (2005), Wildfire-related debris flow from a hazards perspective, 363–385, in *Debris-Flow Hazards and Related Phenomena*, edited by M. Jacob and O. Hungr, Praxis, Springer-Verlag, Berlin.

Cannon, S. H., E. M. Boldt, J. L. Laber, J. W. Kean, and D. M. Staley (2011), Rainfall intensity–duration thresholds for postfire debris-flow emergency-response planning, *Nat. Hazards*, *59*(1), 209–236.

Cannon, S. H., E. R. Bigio, and E. Mine (2001), A process for fire-related debris flow initiation, Cerro Grande fire, New Mexico, *Hydrolog. Processes*, *15*(15), 3011–3023.

Cannon, S. H., J. E. Gartner, M. G. Rupert, J. A. Michael, A. H. Rea, and C. Parrett (2010), Predicting the probability and volume of postwildfire debris flows in the intermountain western United States, *GSA Bull.*, *122*(1–2), 127–144.

Cannon, S. H., J. E. Gartner, R. C. Wilson, J. C. Bowers, and J. L. Laber (2008), Storm rainfall conditions for floods and debris flows from recently burned areas in southwestern Colorado and southern California, *Geomorphology*, *96*(3–4), 250–269.

China, S., C. Mazzoleni, K. Gorkowski, A. C. Aiken, and M. K. Dubey (2013), Morphology and mixing state of individual freshly emitted wildfire carbonaceous particles, *Nat. Comm.*, *4*(2122); doi:10.1038/ncomms3122.

Chong, J., J. Renaud, and E. Ailsworth (2004), Flash floods wash away lives, dreams, *Los Angeles Times* (3 January 2004), B1.

DeGraff, J. V., S. H. Cannon, and A. J. Gallegos (2007), Reducing post-wildfire debris flow risk through the Burned Area Emergency Response (BAER) process, Conference Presentations from 1st North American Landslide Conference, Vail Colorado, AEG Special Publication, 23.

Eidenshink, J., B. Schwind, K. Brewer, Z. Zhu, B. Quayle, and S. Howard (2007), A project for monitoring trends in burn severity, *Fire Ecol.*, *3*(1), 3–21.

Finney, M. A. (2002), Fire growth using minimum travel time methods, *Can. J. For. Res.*, *32* (8), 1420–1424.

Finney, M. A. (2006), FlamMap 3.0. USDA Forest Service, Rocky Mountain Research Station, Fire Sciences Laboratory, Missoula, MT, Rep., USDA Forest Service, Rocky Mountain Research Station, Portland, OR, 213–220.

Finney, M. A., C. W. McHugh, I. C. Grenfell, K. L. Riley, and K. C. Short (2011), A simulation of probabilistic wildfire risk components for the continental United States, *Stochas. Environ. Res. Risk Assess.*, *25*(7), 973–1000.

Finney, M. A., I. C. Grenfell, C. W. McHugh (2009), Modeling containment of large wildfires using generalized linear mixed-model analysis, *For. Sci.*, *55*(3), 249–255.

Finney, M. A., J. D. Cohen, S. S. McAllister, and W. M. Jolly (2012), On the need for a theory of wildland fire spread, *Int. J. Wildland Fire*, *22*(1), 25–36.

Gartner, J. E., S. H. Cannon, E. R. Bigio, N. K. Davis, C. Parrett, K. L. Pierce, M. G. Rupert, B. L. Thurston, M. J. Trebish, S. P. Garcia, and A. H. Rea (2005), Compilation of data relating to the erosive response of 608 recently burned basins in the Western United States, US Geological Survey Open-File Report, 2005–1218.

Haas, J. R., D. E. Calkin, and M. P. Thompson (2013), A national approach for integrating wildfire simulation modeling into wildland urban interface risk assessments within the United States, *Landscape Urb. Plan.*, *119*, 44–53.

Haas, J. R., D. E. Calkin, and M.P. Thompson (2014), Wildfire risk transmission in the Colorado front range, USA, *Risk Anal.*; doi: 10.1111/risa.12270.

Harpold, A. A., J. A. Biederman, K. Condon, M. Merino, Y. Korgaonkar, T. Nan, L. L. Sloat, M. Ross, P. D, Brooks (2014), Changes in snow accumulation and ablation following the Las Conchas forest fire, New Mexico, USA, *Ecohydrology*, *7*(2), 440–452.

Helsel, D. R., and R. M. Hirsch (2002), Statistical methods in water resources, 510, in *Techniques of Water-Resources Investigations of the United States Geological Survey, Book 4, Hydrological Analysis and Interpretation*, Elsevier, Reston, Virginia.

Hyde, K., M. B. Dickinson, G. Bohrer, D. Calkin, L. Evers, J. Gilbertson-Day, T. Nicolet, K. Ryan, and C. Tague (2012), Research and development supporting risk-based wildfire

effects prediction for fuels and fire management: status and needs, *Int. J. Wildland Fire*, *22*(1), 37–50.

Johansen, M. P., T. E. Hakonson, and D. D. Breshears (2001), Postfire runoff and erosion from rainfall simulation: Contrasting forest with shrublands and grasslands, *Hydrolog. Processes*, *15*, 2953–2965.

Jones, O. D., P. Nyman, and G. J. Sheridan (2014), Modelling the effects of fire and rainfall regimes on extreme erosion events in forested landscapes, *Stochas. Environ. Res. Risk Assess.*, *28*, 2015–2025.

Julyan, R. H., and M. Stuever (2005), *Field Guide to the Sandia Mountains*, University of New Mexico Press, Albuquerque, NM.

Keane, R. E., S. A. Mincemoyer, K. M. Schmidt, D. G. Long, and J. L. Garner (2000), Mapping vegetation and fuels for fire management on the Gila National Forest Complex, New Mexico [CD-ROM], Gen. Tech. Rep. RMRS-GTR-46-CD, Ogden, UT, USDA Forest Service, Rocky Mountain Research Station.

Keeley, J. E. (2009), Fire intensity, fire severity and burn severity–A brief review and suggested usage, *Int. J. Wildland Fire*, *18*(1), 116–126.

Keeley, J. E., T. Brenna, and A. H. Pfaff (2008), Fire severity and ecosystem responses following crown fires in California shrublands, *Ecol. Appl.*, *18*(6), 1530–1546.

LANDFIRE (2012), LANDFIRE 1.3 LCP layer, US Department of Interior Geological Survey [Online], http://landfire.cr.usgs.gov/viewer/ (2015, January).

Meyer, G. A., and S. G. Wells (1997), Fire-related sedimentation events on alluvial fans, Yellowstone National Park, USA, *J. Sediment. Res.*, *67*(5), 776–791.

Nature Conservancy (2014), Rio Grande water fund: Comprehensive plan for wildfire and water source protection, accessed 4 September 2013, at http://www.nmconservation.org/RGWF/RGWF_CompPlan.pdf.

Nyman, P., G. J. Sheridan, and P. N. J. Lane (2013), Hydrogeomorphic response models for burned areas and their applications in land management, *Prog. Phys. Geog.*, *37*(6), 787–812.

Parks, S. A., M. Parisien, and C. Miller (2011), Multi-scale evaluation of the environmental controls on burn probability in a southern Sierra Nevada landscape, *Int. J. Wildland Fire*, *20*, 815–828.

Parsons, A., B. Jarvis, and A. Orleman (2002), Mapping of post-wildfire burned severity using remote sensing and GIS, in 22nd Annual Esri Conference, September, 2002: Redlands, CA, Proceedings, Environmental Systems Research Institute, Inc., also available at http://proceedings.esri.com/library/userconf/proc02/pap0431/p0431.htm.

Pyne, S. J., P. L. Andrews, and R. D. Laven (1996), *Introduction to Wildland Fire*, 2 ed., John Wiley and Sons, New York,

Rhoades, C. C., D. Entwistle, D. Butler (2011), The influence of wildfire extent and severity on streamwater chemistry, sediment and temperature following the Hayman Fire, Colorado, *Int. J. Wildland Fire*, *20*(3), 430–442.

Riley, K. L., R. Bendick, K. D. Hyde, and E. J. Gabet (2013), Frequency-magnitude distribution of debris flows compiled from global data, and comparison with post-fire debris flows in the western US, *Geomorphology*, *191*, 118–128.

Rothermel, R. C. (1972), A mathematical model for predicting fire spread in wildland fuels, Res. Pap. INT-115, USDA Forest Service, Intermountain Forest and Range Experiment Station, Ogden, UT.

Scott, J. H., and E. D. Reinhardt (2001), Assessing crown fire potential by linking models of surface and crown fire behavior, Res. Pap. RMRS-RP-29., USDA Forest Service, Rocky Mountain Research Station, Fort Collins, CO.

Scott, J. H., and R. E. Burgan (2005), Standard fire behavior fuel models: A comprehensive set for use with Rothermel's surface fire spread model, Gen. Tech. Rep. RMRS-GTR-153, US Department of Agriculture, Forest Service, Rocky Mountain Research Station, Fort Collins, CO.

Scott, J. H., M. P. Thompson, and J. W. Gilbertson-Day (2015), Exploring how alternative mapping approaches influence fireshed assessment and human community exposure to wildfire, *GeoJournal, 1–15*; doi: 10.1007/s10708-015-9679-6.

Short, K. C. (2013), A spatial database of wildfires in the United States, 1992–2011, *Earth Syst. Sci. Data Discuss.*, *6*(2), 297–366.

Short, K. C. (2014), Spatial wildfire occurrence data for the United States, 1992–2012 (FPA_FOD_20140428) 2nd, USDA Forest Service, Rocky Mountain Research Station, Fort Collins, CO, http://dx.doi.org/10.2737/RDS-2013-0009.

Smith, H. G., G. J. Sheridan, P. N. J. Lane, P. Nyman, and S. Haydon (2011), Wildfire effects on water quality in forest catchments: A review with implications for water supply, *J. Hydrol.*, *396*, 170–192.

Staley, D. M. (2013), Emergency assessment of post-fire debris-flow hazards for the 2013 Rim Fire, Stanislaus National Forest and Yosemite National Park, California: US Geological Survey Open-File Report 2013–1260, http://pubs.usgs.gov/of/2013/1260/.

State of California Sierra Nevada Conservancy (2014), Mokelumne Watershed Avoided Cost Analysis., http://www.sierranevada.ca.gov/our-work/mokelumne-watershed-analysis, last accessed 13 November 2014.

Thompson, M. P., and D. E. Calkin (2011), Uncertainty and risk in wildland fire management: a review, *J. Environ. Man.*, *92*(8), 1895–1909.

Thompson, M. P., J. R. Haas, J. W. Gilbertson-Day, J. H. Scott, P. Langowski, E. Bowne, and D. E. Calkin (2015a), Development and application of a geospatial wildfire exposure and risk calculation tool, *Environ. Mod. Soft.*, *63*, 61–72.

Thompson, M. P., J. Scott, D. Helmbrecht, and D. E. Calkin (2013a), Integrated wildfire risk assessment: Framework development and application on the Lewis and Clark National Forest in Montana, USA, *Integrat. Environ. Assess. Man.*, *9*(2), 329–342.

Thompson, M. P., J. Scott, J. D. Kaiden, and J. W. Gilbertson-Day (2013c), A polygon-based modeling approach to assess exposure of resources and assets to wildfire, *Nat. Hazards*, *67*(2), 627–644.

Thompson, M. P., J. Scott, P. G. Langowski, J. W. Gilbertson-Day, J. R. Haas, and E. M. Bowne (2013b), Assessing watershed-wildfire risks on National Forest System lands in the Rocky Mountain Region of the United States, *Water*, *5*(3), 945–971.

Thompson, M. P., J. W. Gilbertson-Day, and J. H. Scott (2015b), Integrating pixel-and polygon-based approaches to wildfire risk assessment: Application to a high-value watershed on the Pike and San Isabel national forests, Colorado, USA, *Environ. Mod. Assess.,* 1–15.

Tillery, A. C., J. R. Haas, L. W. Miller, J. H. Scott, and M. P. Thompson (2014), Potential postwildfire debris-flow hazards: A prewildfire evaluation for the Sandia and Manzano mountains and surrounding areas, Central New Mexico, US Geological Survey Scientific Investigations Report 2014–5161, http://dx.doi.org/10.3133/sir20145161.

Tillery, A. C., M. J. Darr, S. H. Cannon, and J. A. Michael (2011), Postwildfire preliminary debris flow hazard assessment for the area burned by the 2011 Las Conchas Fire in north-central New Mexico, US Geological Survey Open-File Report 2011–1308.

US Geological Survey and USDA Forest Service (2013), Monitoring Trends in Burn Severity, Fire Level Geospatial Data, MTBS Project accessed June 2013, at http://mtbs.gov/data/individualfiredata.html.

Warziniack, T., and M. Thompson (2013), Wildfire risk and optimal investments in watershed protection, *West. Econ. For.*, *12*(2), 19–28.